Baicalin mitigates polycystic ovary syndrome-associated non-alcoholic fatty liver disease by inhibiting the AR/SREBP1 axis

BI-HUI JIN[1*], HAN XU[1*], ZI-YAN ZHANG[2], YU-HANG FAN[3], CHUN-YAN JIANG[2], SHAO-LONG QI[4], CHEN-YU XIAO[5], XIAO-HUA FU[1] and LING-BO QIAN[2]

[1]Center for Reproductive Medicine, Department of Reproductive Endocrinology, Zhejiang Provincial People's Hospital (Affiliated People's Hospital), Hangzhou Medical College, Hangzhou, Zhejiang 310014, P.R. China; [2]Department of Physiology, School of Basic Medical Sciences and Forensic Medicine, Hangzhou Medical College, Hangzhou, Zhejiang 310053, P.R. China; [3]Department of Reproductive Endocrinology, Center for Reproductive Medicine, The First Affiliated Hospital, Zhejiang University School of Medicine, Hangzhou, Zhejiang 315300, P.R. China; [4]Department of Vascular Surgery, China-Japan Union Hospital of Jilin University, Changchun, Jilin 130031, P.R. China; [5]Center for Reproductive Medicine, Department of Gynecology, Zhejiang Provincial People's Hospital (Affiliated People's Hospital), Hangzhou Medical College, Hangzhou, Zhejiang 310014, P.R. China

Received May 6, 2025; Accepted August 19, 2025

DOI: 10.3892/ijmm.2025.5630

Abstract. Polycystic ovary syndrome (PCOS) is a common endocrine disorder frequently associated with metabolic disturbances, such as non-alcoholic fatty liver disease (NAFLD), driven by hyperandrogenism-induced lipogenesis. Baicalin (BA), a flavonoid derived from *Scutellaria baicalensis*, exhibits therapeutic potential in the treatment of PCOS; however, the specific mechanisms against PCOS-associated NAFLD remain unclear. In the present study, a PCOS mouse model was established via subcutaneous implantation of dihydrotestosterone. Model validation confirmed irregular estrous cycles, ovarian histopathological abnormalities and altered serum hormone levels. Treatment with BA markedly alleviated NAFLD-associated metabolic abnormalities, including central obesity, dyslipidemia and hepatic steatosis. Moreover, liver transcriptomics indicated that BA modulated lipid metabolism primarily through sterol regulatory element-binding protein 1 (SREBP1)-mediated lipogenesis. Results of western blot analysis confirmed that BA suppressed hepatic protein expression of SREBP1 and its downstream lipogenic enzymes, fatty acid synthase and acetyl-CoA carboxylase, indicating inhibition of hepatic lipogenesis. As androgen receptor (AR) functions as an upstream transcriptional regulator of SREBP1, network pharmacological analysis highlighted AR as a potential target of BA. Molecular docking predicted the BA-AR binding site, guiding purification of truncated AR protein for isothermal titration calorimetry (ITC). Subsequently ITC was used to confirm the specific BA-AR binding affinity. Luciferase reporter assays in MDA-kb2 cells demonstrated that BA inhibited AR transcriptional activity. Collectively, the results of the present study indicated that BA ameliorates PCOS-associated NAFLD through targeting the AR/SREBP1 axis, highlighting its potential as a therapeutic strategy for managing lipid metabolism disorders in PCOS.

Correspondence to: Professor Ling-Bo Qian, Department of Physiology, School of Basic Medical Sciences and Forensic Medicine, Hangzhou Medical College, 481 Binwen Road, Hangzhou, Zhejiang 310053, P.R. China
E-mail: bioqian@163.com

Dr Xiao-Hua Fu, Center for Reproductive Medicine, Department of Reproductive Endocrinology, Zhejiang Provincial People's Hospital, (Affiliated People's Hospital), Hangzhou Medical College, 158 Shangtang Road, Hangzhou, Zhejiang 310014, P.R. China
E-mail: fxh9210@163.com

*Contributed equally

Abbreviations: ACC, acetyl-CoA carboxylase; ANOVA, analysis of variance; AR, androgen receptor; BH, Benjamini-Hochberg; BA, baicalin; CO_2, carbon dioxide; DHT, dihydrotestosterone; FASN, fatty acid synthase; FSH, follicle-stimulating hormone; GO, gene ontology; GST, glutathione S-transferase; H&E, hematoxylin and eosin; ITC, isothermal titration calorimetry; KEGG, Kyoto Encyclopedia of Genes and Genomes; LH, luteinizing hormone; NAFLD, non-alcoholic fatty liver disease; NEFA, non-esterified fatty acids; PCOS, polycystic ovary syndrome; PPI, protein-protein interactions; qPCR, quantitative PCR; SD, standard deviation; SREBP1, sterol regulatory element-binding protein 1; TC, total cholesterol; TG, triglycerides

Key words: polycystic ovary syndrome, non-alcoholic fatty liver disease, baicalin, androgen receptor, sterol regulatory element-binding protein 1, lipid metabolism

Introduction

Polycystic ovary syndrome (PCOS) is a common endocrine disorder affecting 6-20% of reproductive-aged females (1). This condition is characterized by hyperandrogenism, insulin resistance and metabolic dysfunction, all of which markedly increase the risk of non-alcoholic fatty liver disease

(NAFLD) (2,3). NAFLD, the most prevalent chronic liver disease worldwide, affects 32.4% of the general population and 25.6% of females. Notably, prevalence of this disease is markedly higher in patients with PCOS (34-70%) compared with the general population (14-34%), with patients experiencing a greater severity of hepatic steatosis and fibrosis (4,5). In addition, PCOS remains an independent risk factor for NAFLD, even after adjusting for body mass index (6). The coexistence of these conditions imposes substantial health and economic burdens, with PCOS alone accounting for ~$8 billion in annual medical costs, in addition to $1,613 per patient with NAFLD (7). Thus, elucidating the mechanisms underlying lipid deposition in PCOS and developing targeted therapeutic strategies to prevent PCOS-associated NAFLD progression are crucial to alleviate these burdens.

The pathophysiological association between PCOS and NAFLD is driven by a complex interplay of hormonal and metabolic factors, with hyperandrogenism playing a central role (2). Elevated androgen levels promote hepatic steatosis through enhancing *de novo* lipogenesis via androgen receptor (AR)-mediated activation of sterol regulatory element-binding protein 1 (SREBP1), which upregulates key lipogenic enzymes, such as fatty acid synthase (FASN) and acetyl-CoA carboxylase (ACC) (8). The role of SREBP1 in NAFLD is well-established (9) and previous studies in PCOS mouse models confirmed that AR-SREBP1 signaling contributes to increased hepatic lipid accumulation (10). These findings suggested that hyperandrogenism is a crucial driver of metabolic dysfunction in PCOS, highlighting that AR inhibition may exhibit potential as a therapeutic target. However, AR inhibitors, such as flutamide and bicalutamide, are often associated with adverse events, and their long-term utility in females remains controversial. Thus, further investigations are required to determine novel AR-targeted strategies that exhibit increased levels of safety and tolerability (11,12).

Despite advances in understanding PCOS-associated NAFLD, effective treatment options remain limited. Current management strategies largely mimic those used for general NAFLD, relying on weight loss and pharmacotherapy (2). However, weight loss, considered the first-line intervention, is often difficult to achieve and maintain due to poor adherence, while pharmacological treatments developed for diabetes and obesity are frequently associated with side effects (13,14). Moreover, hyperandrogenism may reduce the efficacy of these therapies, highlighting the urgent requirement for targeted interventions that address the underlying androgen-driven pathology of NAFLD in PCOS.

Baicalin (BA), a flavonoid derived from the Traditional Chinese Medicinal herb, *Scutellaria baicalensis*, exhibits a broad range of pharmacological activities, including anti-inflammatory, antioxidant, anti-steatotic and hepatoprotective effects (15). In various *in vivo* and *in vitro* models, BA mitigated hepatic injury via suppressing inflammation and oxidative stress, and improving lipid metabolism through reducing cholesterol and free fatty acid accumulation (15,16). Notably, results of previous studies suggest that BA may modulate androgen-dependent pathways, demonstrating potential benefits in benign prostatic hyperplasia (17), prostate cancer (18) and androgenetic alopecia (19). Results of a previous study also indicated that BA may ameliorate high-androgen-induced PCOS symptoms (20); however, research focused on the efficacy in PCOS-associated NAFLD or its specific mechanism of AR inhibition in the context of PCOS remains limited. Compared with existing AR antagonists, BA may offer a more manageable toxicity profile and fewer off-target effects, highlighting its potential for long-term management of androgen-driven pathologies. Notably, the specific anti-androgenic mechanisms underlying BA and the potential impact on hepatic lipid deposition under hyperandrogenic conditions are yet to be fully elucidated.

The present study aimed to investigate the potential impact of BA on the AR/SREBP1 signaling pathway, including the suppression of *de novo* lipogenesis and reductions in hepatic lipid accumulation in PCOS-associated NAFLD. The present study also aimed to validate the specific role of BA in mitigating hyperandrogenism-induced liver damage and to provide novel mechanistic insights into its potential effects on hepatic lipid metabolism under hyperandrogenic conditions. Results of the present study may provide novel insights for the development of targeted therapies and advance the current understanding of innovative treatment strategies for PCOS-associated NAFLD.

Materials and methods

Animal experiments. All animal experiments were approved by the Ethics Committee of Zhejiang Provincial People's Hospital (approval no. 20240708135746975190) and conducted in accordance with the ARRIVE guidelines (21). Two-week-old female C57BL/6J mice (n=52; 5-6 g; Shanghai Laboratory Animals Center) were housed under standard specific pathogen-free conditions (22±2˚C; relative humidity 50±5%; 12-h light/dark cycle) with *ad libitum* access to food and water, and were acclimated for one week. Initially, mice were randomly divided into two groups; namely, a control group (n=14) and a PCOS model group (n=38). Control mice received subcutaneous implants of empty silicone tubes, while PCOS mice received implants containing 10 mg dihydrotestosterone (DHT) (22,23). The tubes were replaced every 4 weeks. After 4 weeks, six mice from each group were sacrificed to confirm successful PCOS modeling via estrous cycle analysis, ovarian hematoxylin and eosin (H&E) staining and serum hormone measurements. The control group included a total of eight mice, each receiving saline. The remaining 32 PCOS mice were randomly divided into four groups (n=8 per group); namely, PCOS group (saline-treated) and three BA treatment groups receiving low (100 mg/kg/day), medium (200 mg/kg/day) or high (400 mg/kg/day) doses of BA orally. DHT implants were continued for both PCOS and BA treatment groups. Notably, treatment was initiated at week 5 and lasted 8 weeks. At the end of the treatment period, all mice were fasted for 12 h and weighed. They were then sacrificed in a carbon dioxide (CO_2) chamber that had not been pre-filled with CO_2, ensuring that animals were initially in ambient air (~0.04% CO_2). Medical-grade CO_2 was then introduced at a displacement rate of 30% of the chamber volume per minute, gradually increasing the concentration to >70% to induce rapid deep anesthesia and death while minimizing distress (24). After complete cessation of respiration, CO_2 flow was maintained for at least 1 min to ensure mortality. Mortality was confirmed by the absence of respiration and other vital signs. Blood,

visceral fat and liver tissues were collected from all animals, and portions of liver tissue were fixed in 4% formalin at room temperature (20-25˚C) for 24-48 h before processing for histological examination. The remaining tissues were snap-frozen in liquid nitrogen and stored at -80˚C for subsequent analyses.

Estrous cycle identification. Each morning at 9:00 AM, 20 μl of saline was injected into the vaginal cavity, spread on a slide and stained with 0.5% methylene blue for 5 min at room temperature (20-25˚C). Estrouscycle stages were classified according to the classic cytological criteria (25).

Serum and hepatic biochemical analysis. Serum and hepatic biochemical parameters were measured using commercially available kits (Nanjing Jiancheng Bioengineering Institute). Serum levels of follicle-stimulating hormone (FSH; cat. no. H101-1-2), luteinizing hormone (LH; cat. no. H206-1-2) and DHT (cat. no. H293-1-2) were determined using enzyme-linked immunosorbent assay kits. Lipid metabolism indices, including non-esterified fatty acids (NEFA; cat. no. A042-2-1), triglycerides (TG; cat. no. A110-1-2), total cholesterol (TC; cat. no. A111-1-2), low-density lipoprotein cholesterol (cat. no. A113-1-2) and high-density lipoprotein cholesterol (cat. no. A112-1-2) in serum, as well as hepatic NEFA, TG and TC, were analyzed using biochemical assay kits, according to the manufacturer's instructions.

Histological examination. One ovary and a portion of liver tissue from each mouse were fixed in 4% formalin at room temperature (20-25˚C) for 24-48 h, dehydrated through a graded ethanol series (75% for 24 h, 90% for 12 h, 95% for 4 h, and 100% for 2 h), cleared in xylene for 1-2 h, embedded in paraffin using a standard embedding station (tissues were oriented in molten paraffin within base molds, gently flattened, covered with labeled cassettes and cooled at -20˚C until solidified), and sectioned into consecutive 3-μm-thick slices for H&E staining. Frozen liver tissues were embedded in optimal cutting temperature compound and sectioned into 8-μm-thick slices using a cryostat. Tissues were stained with Oil Red O at room temperature (20-25˚C) for 10 min to evaluate hepatic lipid deposition.

RNA sequencing analysis in mouse liver tissues. A total of four samples per group (control, model and BA-treated at medium dose) were used for sequencing. Total RNA was extracted using TRIzol® reagent (cat. no. 15596018; Invitrogen; Thermo Fisher Scientific, Inc.) following the manufacturer's procedure. The total RNA quantity and purity were analyzed using Qubit 3.0 (cat. no. Q33216; Thermo Fisher Scientific, Inc.) and Fragment Analyzer 5300 (cat. no. M5311AA; Agilent Technologies). High-quality RNA samples with a RIN number >7.0 were used to construct sequencing libraries. After total RNA extraction, mRNA was purified from 2 μg of total RNA using mRNA Capture Beads 2.0 (cat. no. 12629ES; Yeasen Biotechnology Co., Ltd.) with two rounds of purification. The purified mRNA was fragmented into short fragments using magnesium ions (cat. no. 12340ES97; Yeasen Biotechnology Co., Ltd.) at 94˚C. Then the cleaved RNA fragments were reverse-transcribed to synthesize first-Strand cDNA by Reverse Transcriptase, followed by synthesis of the second-stranded cDNA with *E.coli* DNA polymerase I, RNase H and dUTP Solution (cat. no. 12340ES97; Yeasen Biotechnology Co., Ltd.). An A-base was then added to the blunt ends of each strand, preparing them for ligation with indexed adapters containing a T-base overhang. Dual-index adapters were ligated, and the ligated products were amplified by PCR under the following conditions: Initial denaturation at 98˚C for 1 min; 14 cycles of denaturation at 98˚C for 10 sec; annealing at 60˚C for 30 sec; and extension at 72˚C for 30 sec; followed by a final extension at 72˚C for 5 min. The average insert size for the final cDNA libraries was 400±50 bp. Strand specificity was achieved during PCR amplification utilizing a high-fidelity DNA polymerase that selectively amplifies cDNA strands without U-base. PCR products were purified with Hieff NGS DNA Selection Beads (cat. no. 12601ES75; Yeasen Biotechnology Co., Ltd.). The loading concentration of the final library was about 1.2-1.6 pM. 2x150 bp paired-end sequencing (PE150) was performed on the Illumina Novaseq™ X Plus (LC-Bio Technology CO., Ltd.) following the vendor's recommended protocol.

Raw reads were processed, aligned to the mouse genome (GRCm38) and analyzed using StringTie. Differential expression was assessed with DESeq2 [$|\log_2$(fold change)$|>1.5$; Benjamini-Hochberg (BH)-adjusted $q<0.05$]. Gene Ontology (GO) provides a controlled vocabulary that describes biological processes, molecular functions and cellular components (26). The Kyoto Encyclopedia of Genes and Genomes (KEGG) is a curated database of metabolic and signaling pathways (27). Differentially expressed genes were analyzed for GO and KEGG enrichment with the clusterProfiler R package (version, 3.8.1) (28) using pAdjustMethod='BH' and q-valueCutoff=0.05. Terms with $q<0.05$ and at least three gene hits were considered significant.

Reverse transcription-quantitative (RT-q) PCR. Total RNA from mice liver was extracted using TRIzol® reagent (cat. no. 15596026; Thermo Fisher Scientific, Inc.) following the manufacturer's protocol. cDNA was synthesized using HiScript III RT SuperMix (cat. no. R333-01; Vazyme Biotech Co., Ltd.) according to the supplier's instructions. qPCR was performed on a Thermo Fisher 7500 system using ChamQ Universal SYBR Master Mix (cat. no. Q711-03; Vazyme Biotech Co., Ltd.) with β-actin (Actb) as the internal reference gene. The PCR cycling conditions were as follows: Initial denaturation at 95˚C for 30 sec, followed by 40 cycles of denaturation at 95˚C for 10 sec and annealing/extension at 60˚C for 30 sec. A melting curve analysis was performed to confirm amplification specificity. The primer sequences were as follows: *Actb*, forward: 5'-ACGGCCAGGTCATCACTATTG-3' and reverse, 5'-CAAGAAGGAAGGCTGGAAAAGA-3'; and *Srebp1* forward, 5'-GGAGCCATGGATTGCACATT-3' and reverse, 5'-GGCCCGGGAAGTCACTGT-3'. Relative gene expression levels were calculated using the $2^{-\Delta\Delta Cq}$ method (29). All experiments were independently repeated three times to ensure reproducibility.

Western blot analysis. Tissues were lysed in RIPA buffer (cat. no. P0013B; Beyotime Institute of Biotechnology) supplemented with PMSF (cat. no. ST506; Beyotime Institute of Biotechnology) and protease inhibitor cocktail

(cat. no. HY-K0010; MedChemExpress). Protein concentrations were determined using a BCA assay kit (cat. no P0011; Beyotime Institute of Biotechnology). Equal amounts of protein (10 μg per lane) were separated via 4-12% SDS-PAGE and transferred onto PVDF membranes (cat. no. 1620177; Bio-Rad Laboratories, Inc.). Membranes were blocked in 5% skimmed milk (w/v) in TBS-Tween-20 buffer for 2 h at room temperature, and incubated overnight at 4˚C with primary antibodies against ACTB (cat. no. 81115-1-RR; Proteintech Group, Inc.), SREBP1 (cat. no. ab28481; Abcam), FASN (cat. no. 3180; CST Biological Reagents Co., Ltd.) and ACC (cat. no. 3676; CST Biological Reagents Co., Ltd.). Following primary incubation, membranes were washed and incubated with HRP-conjugated secondary antibody (1:10,000 dilution; cat. no. AS003; ABclonal Technology Co., Ltd.) for 1 h at room temperature. Protein bands were visualized using a chemiluminescence kit (cat. no. 36208ES60; Yeasen Biotechnology Co., Ltd.) and images were obtained using an ImageQuant LAS 4000 system (Cytiva).

Network pharmacological analysis. Potential targets of BA were identified using BATMAN 2.0 (http://bionet.ncpsb.org.cn/batman-tcm/#/home), with criteria of Confidence Score ≥0.8 (LR=48) and Druggable Score ≥0.1. Targets were curated and standardized to *Homo sapiens* via UniProt (https://www.uniprot.org/). Disease-associated targets were retrieved from GeneCards (https://www.genecards.org/, version 5.21; with relevance Score >20), OMIM (https://www.omim.org/) and DrugBank (https://go.drugbank.com/, version 5.1.12). All databases were accessed in September 2024. Targets were standardized, merged and de-duplicated. A Venn diagram identified overlapping genes between BA targets and disease-associated targets. Protein-protein interactions were analyzed using STRING (https://string-db.org/), and network visualization was performed in Cytoscape (version, 3.7.2), with node size and color indicating interaction density. The cytoHubba plugin and DMNC algorithm extracted the top 10 hub genes, forming a subnetwork for further analysis.

Molecular docking. The 3D structure of human AR (PDB ID: 2pnu) was retrieved from the Protein Data Bank (www.rcsb.org) and visualized using PyMOL 2.3.0 (Schrödinger, LLC). The 3D structures of BA and flutamide were downloaded as SDF files from PubChem (https://pubchem.ncbi.nlm.nih.gov/) and imported into ChemDraw 2014 (PerkinElmer, Inc.). Energy minimization was performed using the MM2 module to obtain stable conformations, saved as Mol2 files. Ligand and receptor preparations were performed using MGLTools (version, 1.5.6; The Scripps Research Institute), followed by molecular docking with AutoDock Vina 1.1.2 (The Scripps Research Institute). Top-scoring conformations were visualized using PyMOL (version, 2.3.0; https://pymol.org/) and Discovery Studio 2019 (BIOVIA; Dassault Systèmes).

Protein expression and purification. Molecular docking revealed that BA may interact with AR residues 704-899. To obtain the corresponding protein region, a truncated human AR fragment (residues 600-900) was amplified using specific primers (forward, 5'-AATGATTGCACTATTGATAAATTCCG-3' and reverse, 5'-GATGATCTCTGCCATCATTTC-3'), cloned into the pGEX4T1 vector, and transformed into *Escherichia coli* Tuner (DE3) cells (cat. no. D1091S; Beyotime Institute of Biotechnology). Expression of the recombinant GST-tagged AR protein was induced with 0.5 mM IPTG (cat. no. A100487-0025; Sangon Biotech Co., Ltd.) at 16˚C for 16-20 h. Following centrifugation, the bacterial cells were resuspended in Binding/Wash Buffer (pH 7.3-7.5) for GST-Sefinose Resin (cat. no. C600326-0500; Sangon Biotech Co., Ltd.). The buffer was supplemented with 0.2 mg/ml lysozyme (cat. no. L1080; Beijing Solarbio Science & Technology Co., Ltd.), 20 μg/ml DNase I (cat. no. D7073; Beyotime Institute of Biotechnology), 1 mM $MgCl_2$ (cat. no. 7786-30-3; Macklin Biochemical Co., Ltd.), and 1 mM PMSF (cat. no. ST506; Beyotime Institute of Biotechnology). Cell lysis was performed using ultrasonication (60% amplitude, 5 sec on/5 sec off, 4˚C, 20 min), followed by centrifugation at 12,000 x g for 20 min at 4˚C. The clarified supernatant was filtered and subjected to affinity purification using a GST 4FF-tagged protein purification kit (cat. no. C600327-001; Sangon Biotech Co., Ltd.) according to the manufacturer's instructions. The GST-AR fusion protein was eluted in 2 ml fractions with Elution Buffer (pH 7.9~8.1) for GST-Sefinose™ Resin (cat. no. C600325; Sangon Biotech) and analyzed by sodium dodecyl sulfate-polyacrylamide gel electrophoresis (SDS-PAGE).

SDS-PAGE and protein quantification. The purified protein sample was separated on a 10% SDS-polyacrylamide gel alongside bovine serum albumin (BSA) standards ranging from 0.5-10 μg (cat. no. ST023-50 g; Beyotime Institute of Biotechnology). A volume of 10 μl was loaded per lane for both the sample and standards. Following electrophoresis, the gel was stained with Coomassie Brilliant Blue (cat. no. E607056-0250; Sangon Biotech Co., Ltd.) at room temperature for 20 min and destained in double-distilled water for 6 h with changes every 1-2 h. Protein bands were visualized using a gel imaging system (model DH200; Ruicheng Instruments Co., Ltd.) and band intensity was quantified using ImageJ software (version 1.8.0.345; National Institutes of Health) to estimate the concentration of the target protein.

Isothermal titration calorimetry (ITC) analysis. ITC analysis was performed following modifications from previously established methods (30). A 300-μl solution of AR-GST fusion protein (1 μM in PBS; pH 7.4; 1% DMSO) was loaded into the ITC 200 instrument (MicroCal), and equilibrated at 25˚C with stirring at 1,000 rpm for 30 min. A 60-μl BA solution (20 μM in PBS; pH 7.4; 1% DMSO) was injected 21 times (2 μl each time) at 180-sec intervals. Data were analyzed using PEAQ-ITC software (MicroCal) to determine binding constant (K), stoichiometry (n), enthalpy change (ΔH) and entropy change (ΔS). A control titration with GST-only solution was performed under identical conditions.

Androgen receptor transcriptional activity assay. The MDA-kb2 cell line, derived from MDA-MB-453 cells and stably transfected with an MMTV-luciferase reporter driven by androgen response elements, was kindly provided by Professor Wei Shi (School of the Environment, Nanjing

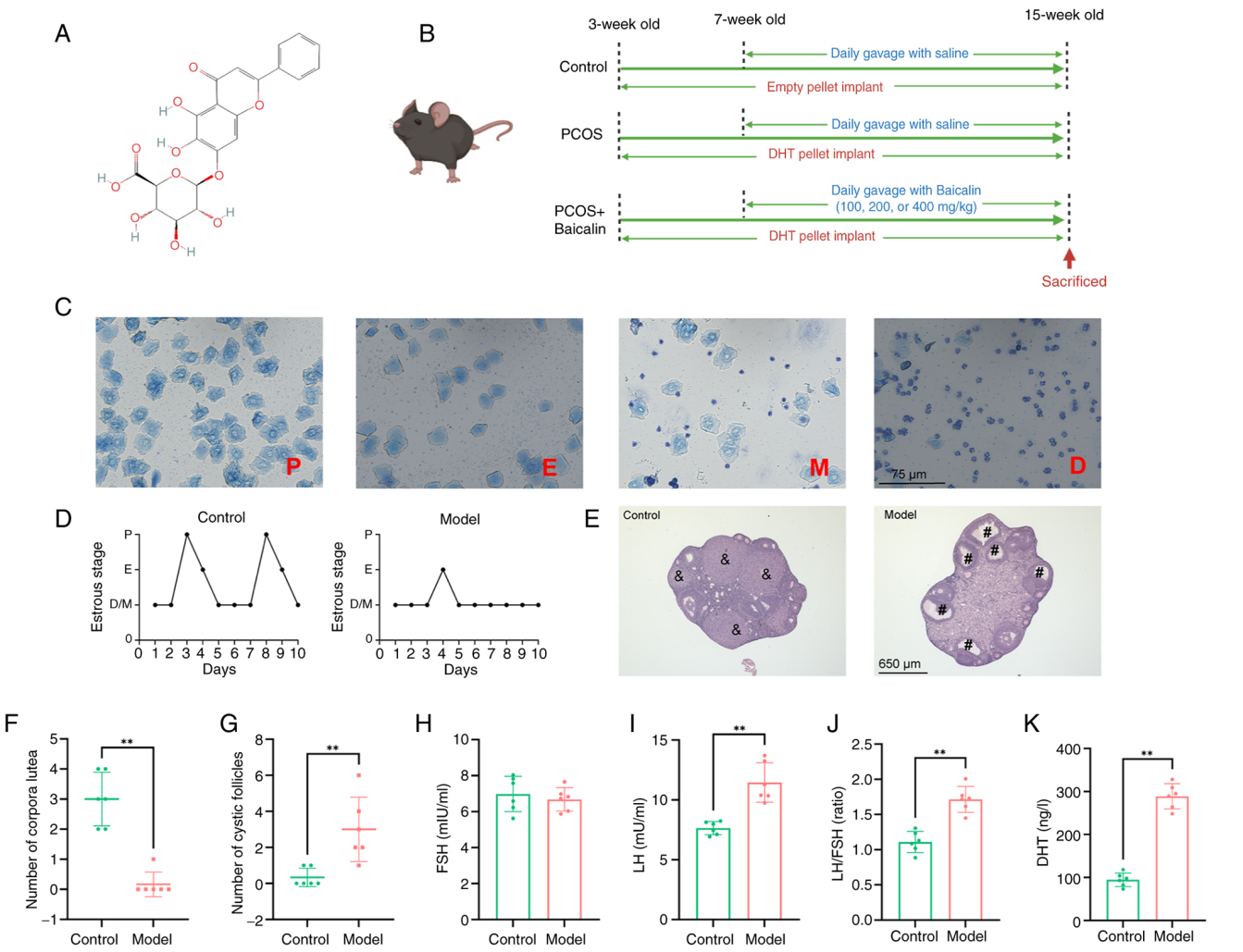

Figure 1. Validation of the PCOS mouse model. (A) Chemical structure of BA. (B) The experimental workflow for animal studies. (C) Representative images of vaginal exfoliated cells in control mice at different estrous cycle stages. Proestrus, predominantly nucleated epithelial cells (single or clustered) with few leukocytes; estrus, large, anucleated, keratinized squamous cells with irregular edges and minimal leukocyte presence; metestrus, reduced keratinized epithelial cells accompanied by numerous leukocytes and nucleated epithelial cells; diestrus, dominated by leukocytes. (D) Representative estrous cycle patterns in control and PCOS mice. (E) Representative ovarian sections stained with H&E. Corpus luteum is indicated by & and cystic follicles are indicated by #. Quantitative comparison of (F) corpora lutea and (G) cystic follicles in control and PCOS groups. Serum levels of (H) FSH, (I) LH, (J) DHT and (K) LH/FSH ratio in control and PCOS groups. Data are presented as the mean ± standard deviation (n=6). **P<0.01. Statistical significance was determined using an unpaired twotailed Student's ttest. PCOS, polycystic ovary syndrome; BA, baicalin; H&E, hematoxylin and eosin; FSH, follicle-stimulating hormone; LH, luteinizing hormone; DHT, dihydrotestosterone.

University, China). This reporter cell line was used to screen AR-regulating compounds. Cells were cultured in Leibovitz's L-15 medium (cat. no. PM151010; Procell Biotechnology Co., Ltd.) with 10% FBS (cat. no. 10099141C; Gibco; Thermo Fisher Scientific, Inc.) and 1% penicillin-streptomycin (cat. no. C0222; Beyotime Institute of Biotechnology) at 37˚C under non-CO_2 conditions. For assays, FBS was replaced with detection medium containing 10% charcoal-stripped serum (cat. no. C3830-0050; VivaCell Bioscientific, Ltd.). Cells were seeded in 96-well plates at a concentration of $3.0x10^5$ cells/ml, incubated for 24 h at 37˚C and subsequently treated with test compounds for an additional 24 h. Following washing with PBS, 50 μl of Steady Glo® reagent (cat. no. E2510; Promega Corporation) was added, and luminescence was measured using a Berthold Junior LB9509 luminometer. AR antagonistic effects of BA (1-30 μM) were quantified as the percentage of luminescence relative to the control treated with 1 nM DHT.

Statistical analysis. Experimental data were analyzed using GraphPad Prism (version, 9; Dotmatics). Data are presented as the mean ± standard deviation (SD). Comparisons between two groups were performed using unpaired Student's t-tests, and comparisons between multiple groups were performed using one-way analysis of variance (ANOVA) followed by Tukey's post hoc test. P<0.05 was considered to indicate a statistically significant difference.

Results

Validation of the PCOS mouse model. The chemical structure of BA and the experimental workflow for animal studies are illustrated in Fig. 1A and B, respectively. Prior to evaluating the therapeutic effects of BA in PCOS mice, the PCOS model established via subcutaneous implantation of DHT was validated. From Day 19 post-implantation, vaginal epithelial cell smears were collected daily to monitor estrous cycle changes.

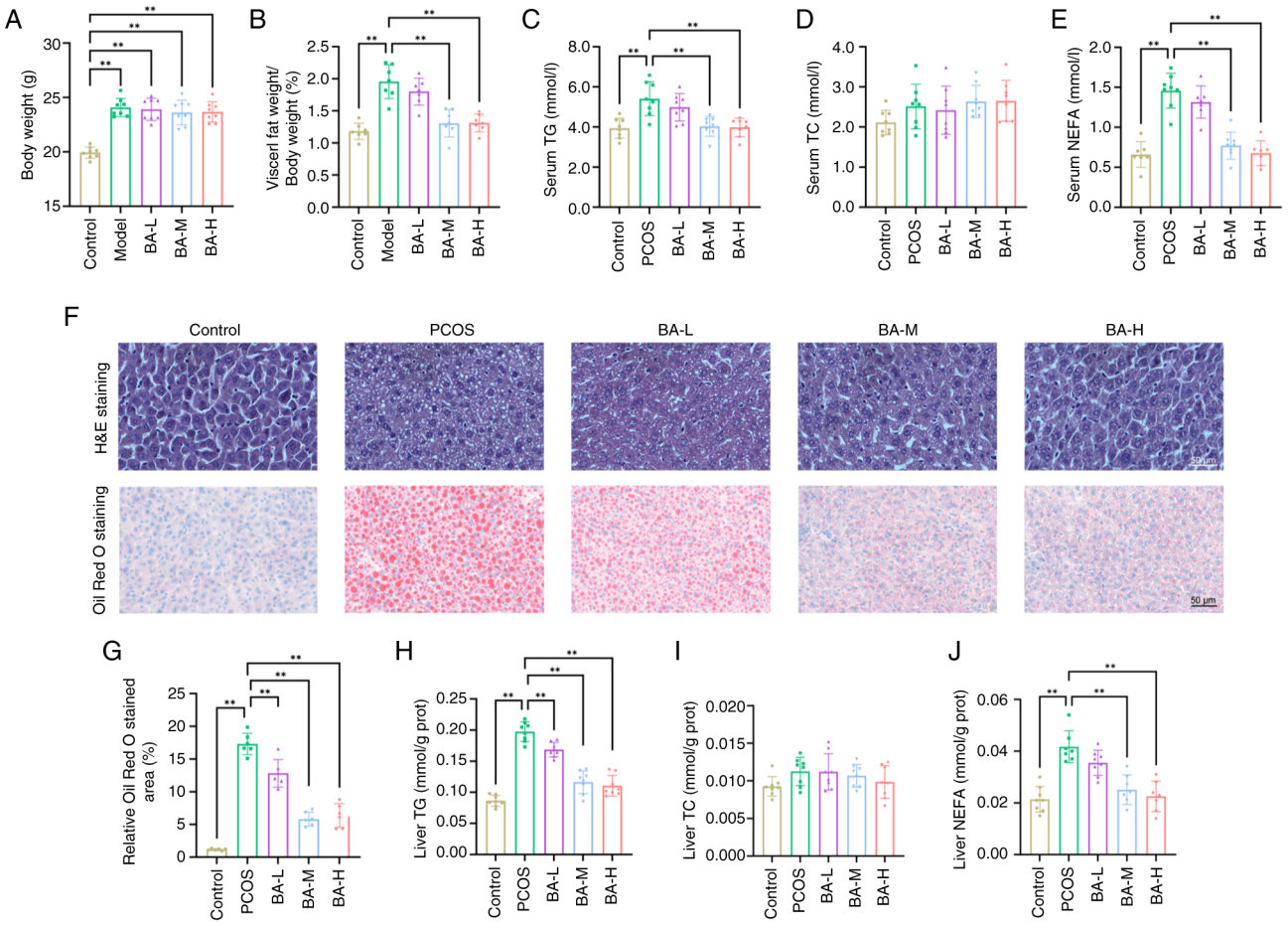

Figure 2. BA treatment alleviates NAFLD-associated features in PCOS mice. (A) Body weight, (B) visceral fat-to-body weight ratio, serum levels of (C) TG, (D) TC and (E) NEFA in each group. (F) Representative liver histology in each group. (G) Quantitative analysis of Oil Red O-positive areas in liver sections. Hepatic levels of (H) TG, (I) TC and (J) NEFA in each group. Data are presented as the mean ± standard deviation (n=6-8). **P<0.01. Statistical significance was assessed using oneway ANOVA followed by Tukey's post hoc test. BA, baicalin; NAFLD, non-alcoholic fatty liver disease; PCOS, polycystic ovary syndrome; TG, triglycerides; TC, total cholesterol; NEFA, non-esterified fatty acids.

Representative cytological features of different estrous stages in control mice are shown in Fig. 1C. Specifically, proestrus is marked by clusters of nucleated epithelial cells, estrus by large anucleated squamous cells, metestrus by a mixed population of epithelial cells and leukocytes, and diestrus by leukocyte predominance. As shown in Fig. 1D, control mice exhibited regular estrous cycles, whereas PCOS mice predominantly remained in diestrus or metestrus, characterized by a predominance of leukocytes in vaginal smears. Ovarian H&E staining revealed a reduction in corpus luteum formation and an increase in cystic follicles in PCOS mice (Fig. 1E-G). In addition, serum analysis demonstrated elevated DHT and LH levels, as well as a markedly increased LH/FSH ratio in PCOS mice (Fig. 1I-K). These findings confirmed that subcutaneous implantation of DHT successfully replicated key pathological features of clinical PCOS, establishing a robust model for subsequent experiments.

BA ameliorates NAFLD-associated metabolic abnormalities in PCOS mice. Results of the present study revealed that body weight, central obesity and dyslipidemia were markedly increased in DHT-induced PCOS mice, as evidenced by elevated serum TG and NEFA (Fig. 2A-E). Excessive hepatic lipid accumulation was confirmed via lipid vacuoles in liver tissues, and elevated hepatic TG and NEFA levels (Fig. 2F-J). BA treatment did not markedly reduce overall body weight; however, results of the present study revealed that visceral fat-to-body weight ratio was markedly decreased, particularly in BA-M and BA-H groups (Fig. 2B). BA also markedly reduced serum TG and NEFA levels (Fig. 2C-E), mitigated hepatic lipid deposition and improved liver architecture (Fig. 2F). In the BA-M and BA-H groups, Oil Red O-positive areas and hepatic TG and NEFA levels were markedly lower than in untreated PCOS mice (Fig. 2G-J). Collectively, these results suggested that BA may exhibit potential in alleviating dyslipidemia and reducing hepatic lipid accumulation, highlighting the potential role as an early intervention treatment strategy for the prevention of PCOS-associated NAFLD progression.

BA alters transcriptomic profiles associated with lipid metabolism in the liver of PCOS mice. Reference-based transcriptome sequencing was performed on liver tissues to elucidate the specific mechanisms underlying BA treatment. Principal component analysis revealed that clustering in the BA-treated group was comparable with the control group (Fig. 3A). Differential gene expression analysis identified 430 upregulated and 819 downregulated genes in PCOS

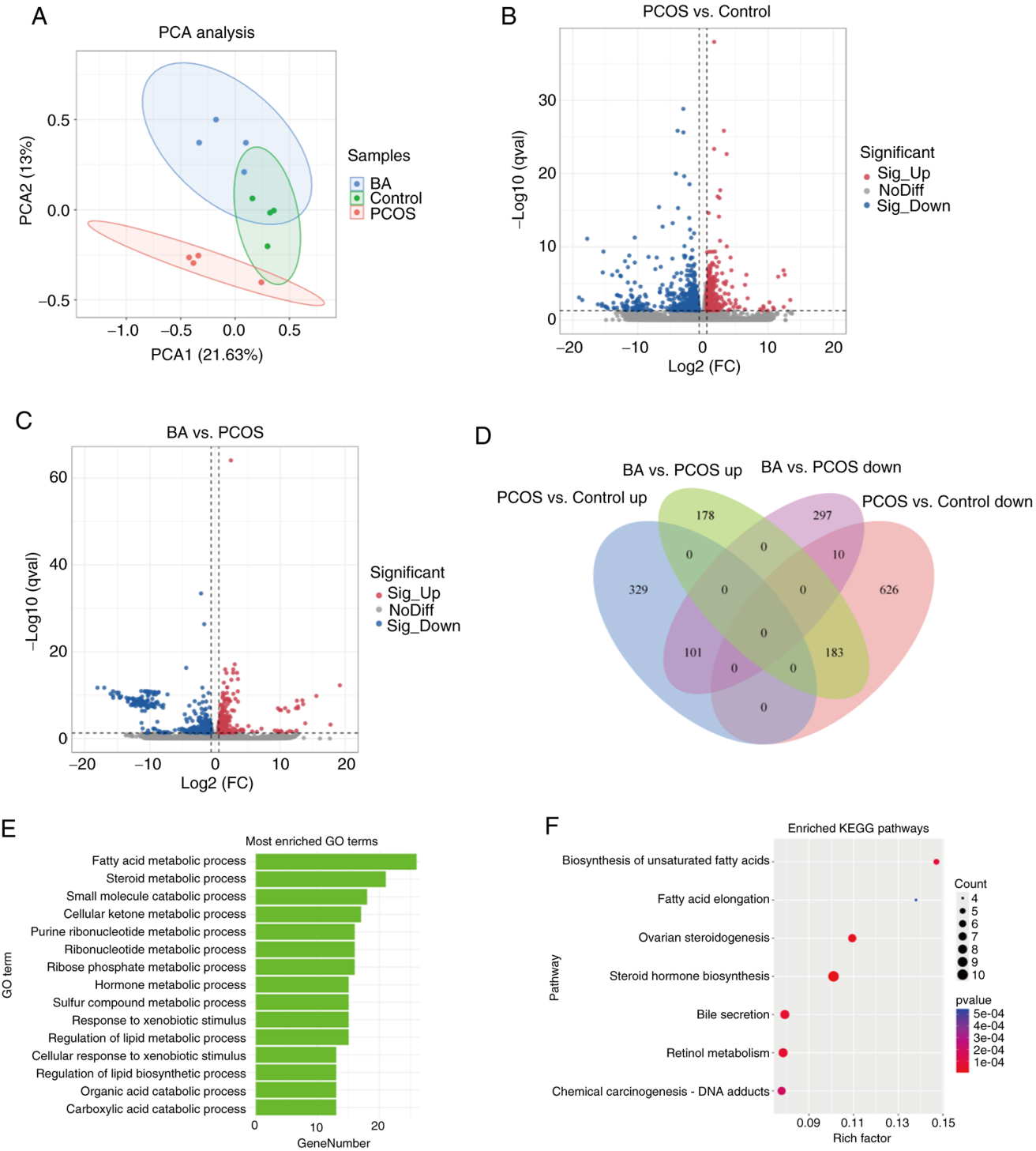

Figure 3. BA modulates lipid metabolism-associated transcriptomic profiles in the liver of PCOS mice. (A) PCA revealed distinct clustering of samples from control, PCOS and BA treatment groups. Volcano plots depicted DEGs between (B) PCOS vs. control and (C) BA-treated vs. PCOS groups. (D) Venn diagram illustrated overlapping DEGs in each group. DEGs were defined by DESeq2 with $|\log_2(\text{fold change})|>1.5$ and BH-adjusted $q<0.05$. (E) GO enrichment analysis of overlapping DEGs highlighted the top 15 enriched biological processes associated with lipid metabolism. (F) KEGG pathway enrichment analysis of overlapping DEGs identified key pathways modulated by BA. GO and KEGG enrichment was assessed using the default hypergeometric test in clusterProfiler, followed by BH-adjusted $q<0.05$. BA, baicalin; PCOS, polycystic ovary syndrome; PCA, principal component analysis; DEGs, differentially expressed genes; BH, Benjamini-Hochberg; GO, Gene Ontology; KEGG, Kyoto Encyclopedia of Genes and Genomes.

mice compared with controls (Fig. 3B), while BA treatment resulted in 361 upregulated and 408 downregulated genes compared with the PCOS model (Fig. 3C). Venn diagram analysis (Fig. 3D) revealed 284 genes as potential therapeutic targets of BA, including 183 genes that were downregulated in PCOS and upregulated by BA, and 101 genes that were upregulated in PCOS and downregulated by BA. GO enrichment analysis (Fig. 3E) revealed that these 284 genes were primarily associated with lipid metabolism, including fatty acid metabolic process, lipid metabolism regulation and lipid biosynthesis. KEGG pathway analysis (Fig. 3F) further highlighted the involvement of BA in modulating lipid metabolism,

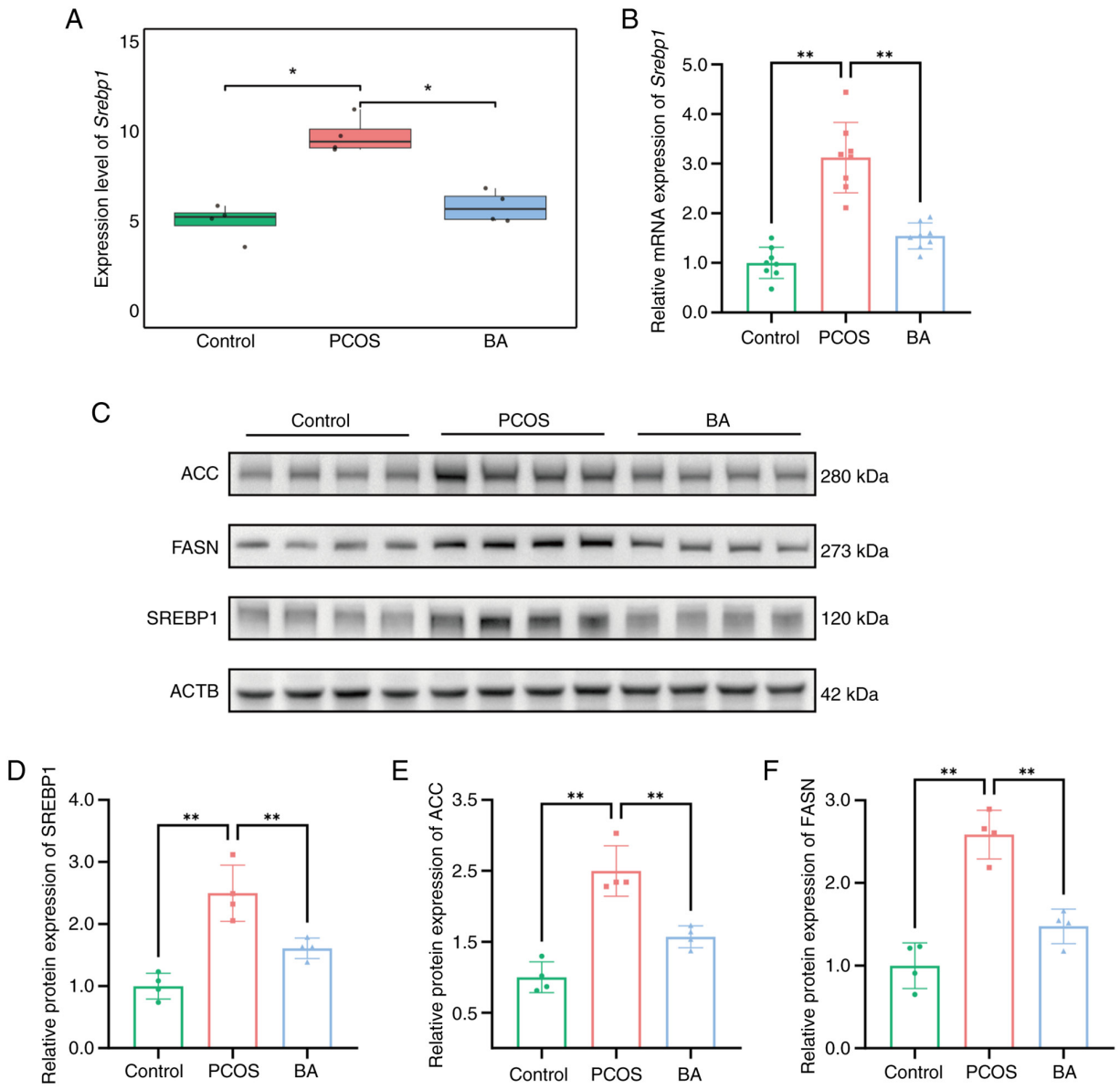

Figure 4. BA regulates *de novo* lipogenesis in PCOS mice through modulating the SREBP1 signaling pathway. (A) Transcriptomic analysis of *Srebp1* gene expression levels in liver tissues (n=4). (B) Relative mRNA expression of *Srebp1* determined using qualitative PCR (n=8). (C) Western blot analysis of SREBP1, ACC and FASN levels in the liver tissue. Quantitative analysis of (D) SREBP1, (E) ACC and (F) FASN protein expression levels. Data are presented as the mean ± standard deviation. *P<0.05, **P<0.01. Statistical significance was assessed using oneway ANOVA followed by Tukey's post hoc test. BA, baicalin; PCOS, polycystic ovary syndrome; *Srebp1, sterol regulatory element-binding protein 1;* ACC, acetyl-CoA carboxylase; FASN, fatty acid synthase.

particularly through pathways associated with unsaturated fatty acid biosynthesis and fatty acid elongation. Collectively, these findings suggested that BA may exert therapeutic effects in PCOS-associated NAFLD through the regulation of fatty acid metabolism.

BA modulates de novo lipogenesis in PCOS mice via the SREBP1 signaling pathway. Genes enriched in GO terms associated with fatty acid metabolic processes, lipid metabolism regulation and lipid biosynthesis regulation were analyzed to investigate the effects of BA on lipid metabolism. Among these, the *Srebp1* gene emerged as a key target that was enriched across all three pathways (Table SI). SREBP1 is a key regulator of *de novo* lipogenesis, controlling genes involved in triglyceride and cholesterol biosynthesis (8). Dysregulated SREBP1 signaling is strongly associated with NAFLD and hepatocellular carcinoma (9). Moreover, SREBP1 is highly expressed in the liver, white adipose tissue and skeletal muscle (31), where it regulates the expression of ACC and FASN. Notably, these enzymes are critical for fatty acid and triglyceride synthesis (9).

To further verify the effects of BA on SREBP1, *Srebp1* expression was examined in the present study. Transcriptomic data revealed that *Srebp1* expression was markedly upregulated in PCOS mice; however, expression levels were markedly attenuated following BA treatment (Fig. 4A). These findings were further confirmed via RT-qPCR analysis (Fig. 4B). In addition, results of the western blot analysis demonstrated that hepatic SREBP1, ACC and FASN were markedly elevated in PCOS mice; however, expression levels were markedly downregulated following BA treatment (Fig. 4C-F). These results indicated that BA may mitigate aberrant *de novo* lipogenesis

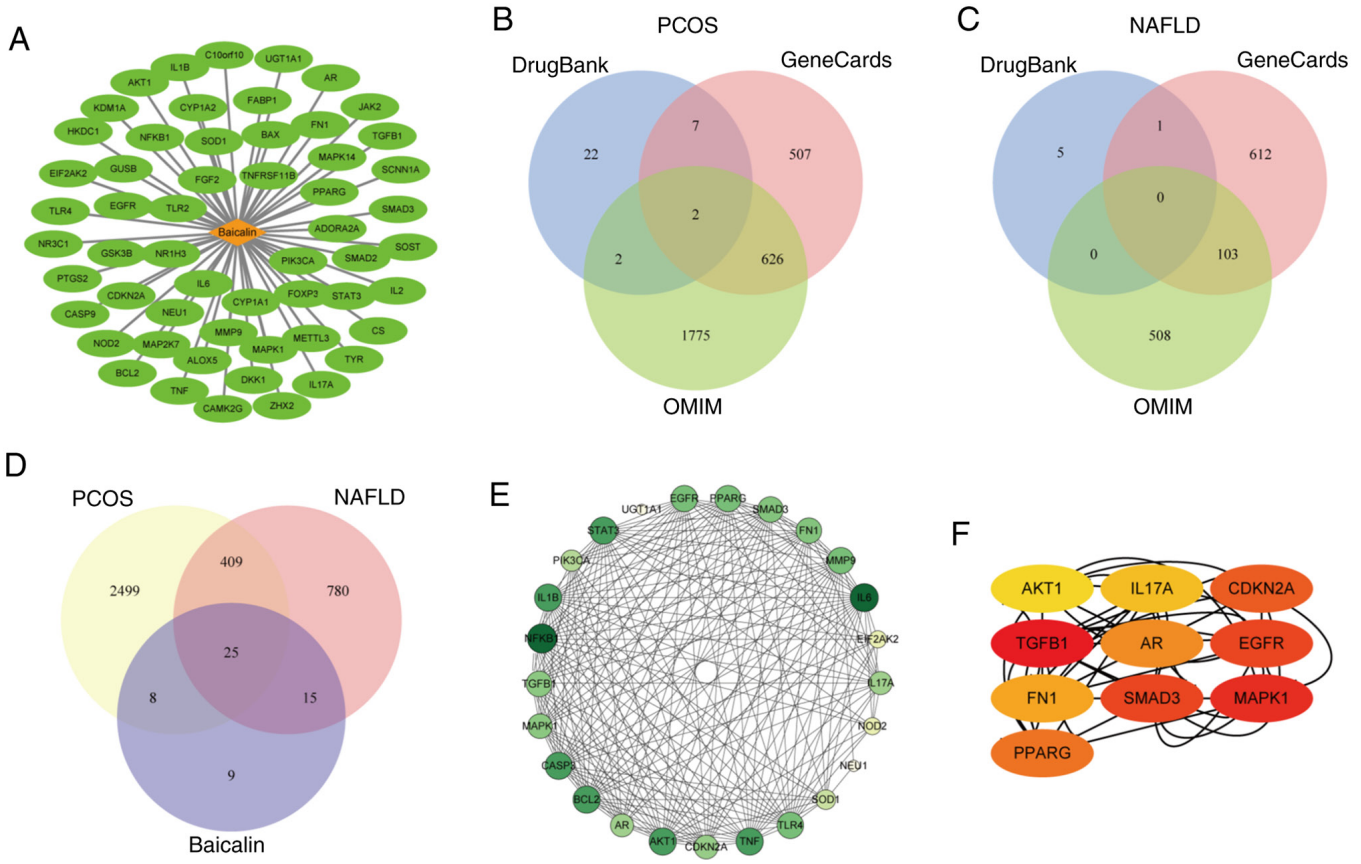

Figure 5. Identification and analysis of therapeutic targets of BA for PCOS-associated NAFLD. (A) BATMAN-TCM identified potential drug targets of BA. GeneCards, OMIM and DrugBank identified disease-associated targets for (B) PCOS and (C) NAFLD. (D) Venn diagram illustrated the overlapping targets among PCOS, NAFLD and BA. (E) PPI network of 25 common genes identified in the Venn diagram. (F) CytoHubba analysis identified the top 10 core genes. BA, baicalin; PCOS, polycystic ovary syndrome; NAFLD, non-alcoholic fatty liver disease; PPI, protein-protein interaction.

in PCOS mice through downregulating the SREBP1 signaling pathway.

Identification of AR as a direct target of BA in PCOS-associated NAFLD. Results of the present study revealed that BA modulated SREBP1; however, it remained unclear whether SREBP1 was a direct target of BA. Thus, a network pharmacological analysis was conducted to identify potential direct targets of BA in PCOS-associated NAFLD. Notably, BATMAN-TCM analysis identified 57 potential BA targets (Fig. 5A). GeneCards, OMIM and DrugBank yielded 2,941 PCOS-associated and 1,229 NAFLD-associated targets (Fig. 5B and C; Table SII). In addition, Venn diagram analysis revealed 25 overlapping genes (Fig. 5D). PPI network analysis (Fig. 5E) and CytoHubba analysis identified 10 core genes, with AR exhibiting potential as a candidate for direct binding (Fig. 5F). Notably, results of a previous study indicated that AR directly binds to the *Srebp1* regulatory region, enhancing transcription (32). Collectively, these findings suggested that BA may exert its therapeutic effects on PCOS-associated NAFLD via the direct targeting of AR and modulation of the AR/SREBP1 pathway.

Direct interaction between BA and AR. Natural compounds often exert their biological effects through interacting with core functional molecules in the body (33,34). However, whether BA exerts therapeutic effects through direct binding to AR remained to be fully elucidated. Thus, molecular docking was performed in the present study to predict the binding affinity and binding sites of BA with AR, comparing these with those of flutamide, a well-established AR antagonist. Results of the present study revealed that the binding energy of BA was -7.5 kcal/mol, which was comparable with that of flutamide at -8.1 kcal/mol. This indicated stable binding, as values below -7.0 kcal/mol are indicative of high-affinity interactions (35). In addition, BA and flutamide exhibited significant structural overlap (Figs. S1; 6A and B). Results of the present study also revealed that BA may form hydrogen bonds with AR residues; namely, LEU704, ASN705 and MET745, at distances of 2.7, 2.8 and 3.0 Å, respectively. Notably, the phenyl ring of BA engaged in pi-alkyl interactions with hydrophobic residues; namely, ILE898 and ILE899, while its hydroxyl group and phenyl ring participated in sulfur/pi-sulfur interactions with MET787, MET742 and MET895. These findings indicated that BA binds to AR in a stable manner.

Based on results of the molecular docking analysis, the pGEX4T1-AR plasmid was designed and constructed using amino acids 600-900 of the human AR protein as a template (Fig. 6C). This plasmid was expressed in prokaryotic cells, and GST-AR fusion protein and AR recombinant protein (truncated AR) were purified via GST affinity chromatography. Coomassie Brilliant Blue staining confirmed the purified proteins (Fig. 6D). Theoretical predictions indicated that the molecular weights of the GST-AR fusion protein and the AR

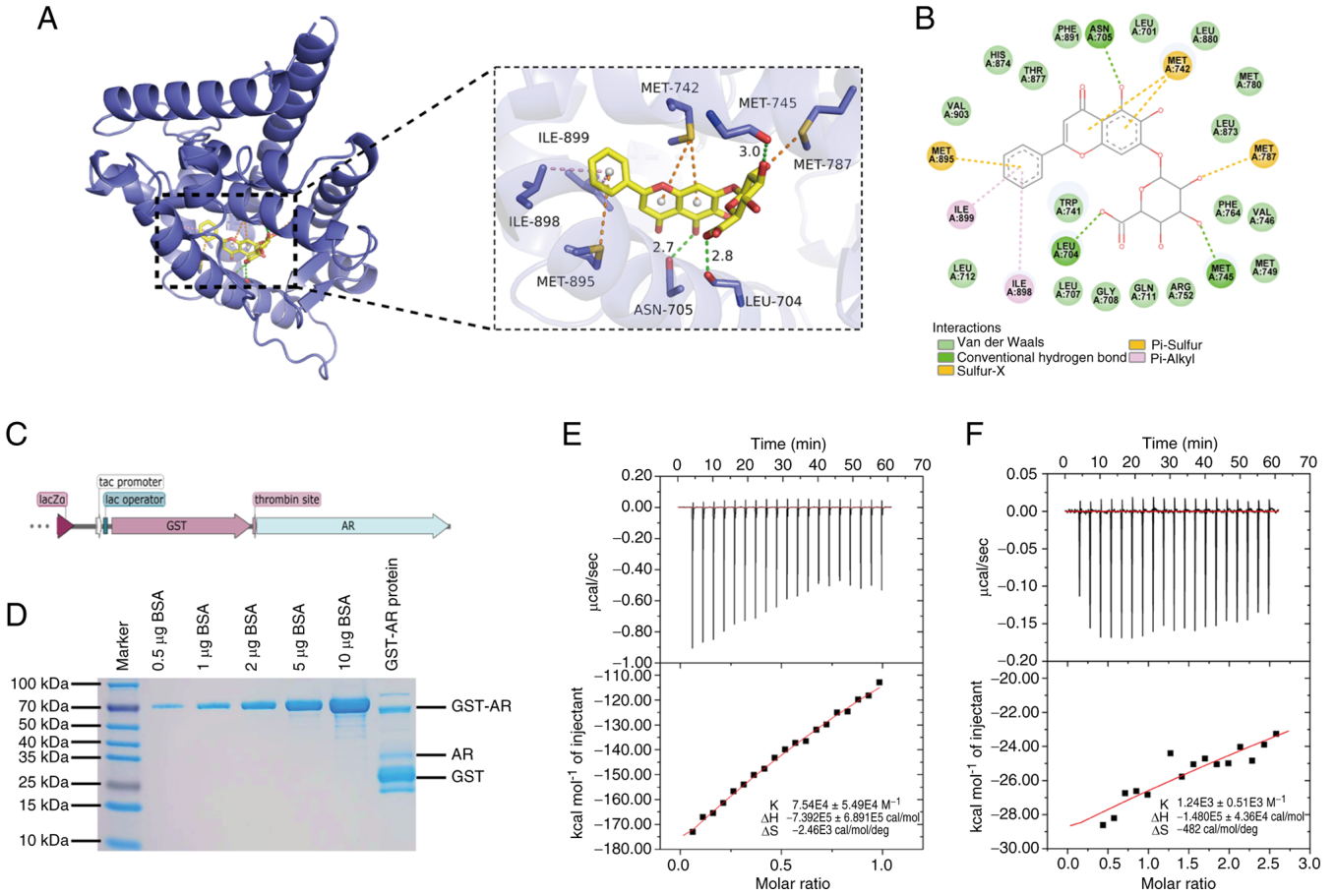

Figure 6. Molecular docking, protein purification and ITC analysis reveal binding between BA and AR. Molecular docking analysis illustrated (A) 2D and (B) 3D binding interactions between BA and AR. (C) Structural diagram of the pGEX4T1-AR plasmid, with the sequence from the N-terminal to C-terminal consisting of a GST tag, restriction sites and the truncated AR protein. (D) GST-AR protein purification and Coomassie Brilliant Blue staining for identification. The order of the samples is indicated at the top of the image. The last lane contains the purified GST-AR protein. ITC analysis of BA binding to a truncated AR protein in (E) sample cells containing 1 μM AR protein (GST-tagged) and in (F) sample cells containing 1 μM GST protein (control). Upper panels, heat flow vs. time; lower panels, normalized heat effects vs. ligand-to-protein molar ratio. ITC, isothermal titration calorimetry; BA, baicalin; AR, androgen receptor; BSA, bovine serum albumin; GST, glutathione S-transferase.

recombinant protein should be ~60 and 35 kDa, respectively, which was consistent with the observed results. Thus, the purification and identification process used in the present study was considered accurate.

To further confirm the direct interaction between BA and AR, ITC was performed in the present study. The binding constant of BA to GST-AR was (7.54±5.49)x10^4 M^{-1} (Fig. 6E), while the binding constant to GST (control) was markedly lower, at (1.24±0.51)x10^3 M^{-1} (Fig. 6F). The ~70-fold higher level of binding to AR indicated a stable and specific interaction, confirming AR as a key target of BA. These results may provide novel insights into the direct binding of BA to AR, highlighting its potential role in modulating AR-associated biological functions.

BA directly binds to AR and inhibits AR transcriptional activity. As AR functions as a transcription factor, the present study aimed to investigate whether BA modulates AR transcriptional activity using MDA-kb2 cells, which contain an MMTV-luciferase reporter driven by AREs (36). Notably, DHT (0-10 nM) induced a dose-dependent increase in AR activity, reaching saturation at 1 nM (Fig. 7A). Results of luciferase assays demonstrated that BA inhibited DHT-induced AR activity in a dose-dependent manner, with 25 μM BA reducing AR transcriptional activity by 80% (Fig. 7B). These findings suggested that BA stably binds to AR with high specificity and antagonizes AR transcriptional activity in a dose-dependent manner. As AR activation promotes SREBP1-driven lipogenesis, BA-mediated inhibition of AR and its downstream target, SREBP1, exhibit potential as a therapeutic strategy for PCOS-associated NAFLD.

Discussion

Results of the present study demonstrated that BA mitigates PCOS-associated NAFLD through antagonizing AR signaling and downregulating the AR/SREBP1 axis. *In vivo*, BA reduced visceral adiposity, serum lipid levels and hepatic lipid accumulation, while restoring the expression of key genes involved in lipid metabolism. *In vitro*, molecular docking and ITC confirmed the high-affinity binding of BA to AR, and results of a functional assay demonstrated the dose-dependent inhibition of AR transcriptional activity. Collectively, these findings highlighted direct AR antagonism as a key mechanism by which BA alleviates PCOS-associated NAFLD.

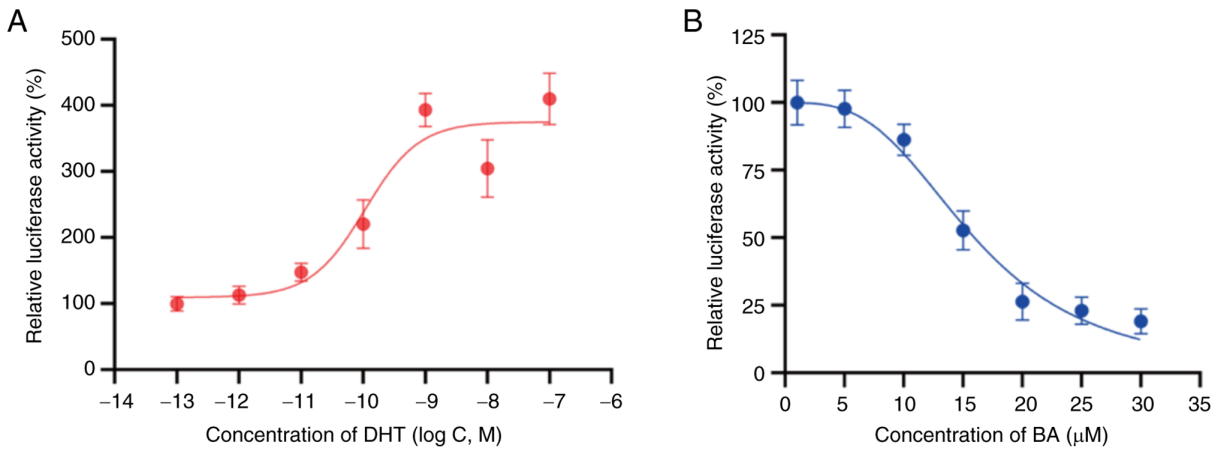

Figure 7. BA inhibits AR transcriptional activity in MDA-kb2 cells. Results of the luciferase reporter assay revealed (A) AR activation through increasing DHT concentrations and (B) BA-mediated AR inhibition in the presence of 1 nM DHT in MDA-kb2 cells. BA, baicalin; AR, androgen receptor; DHT, dihydrotestosterone.

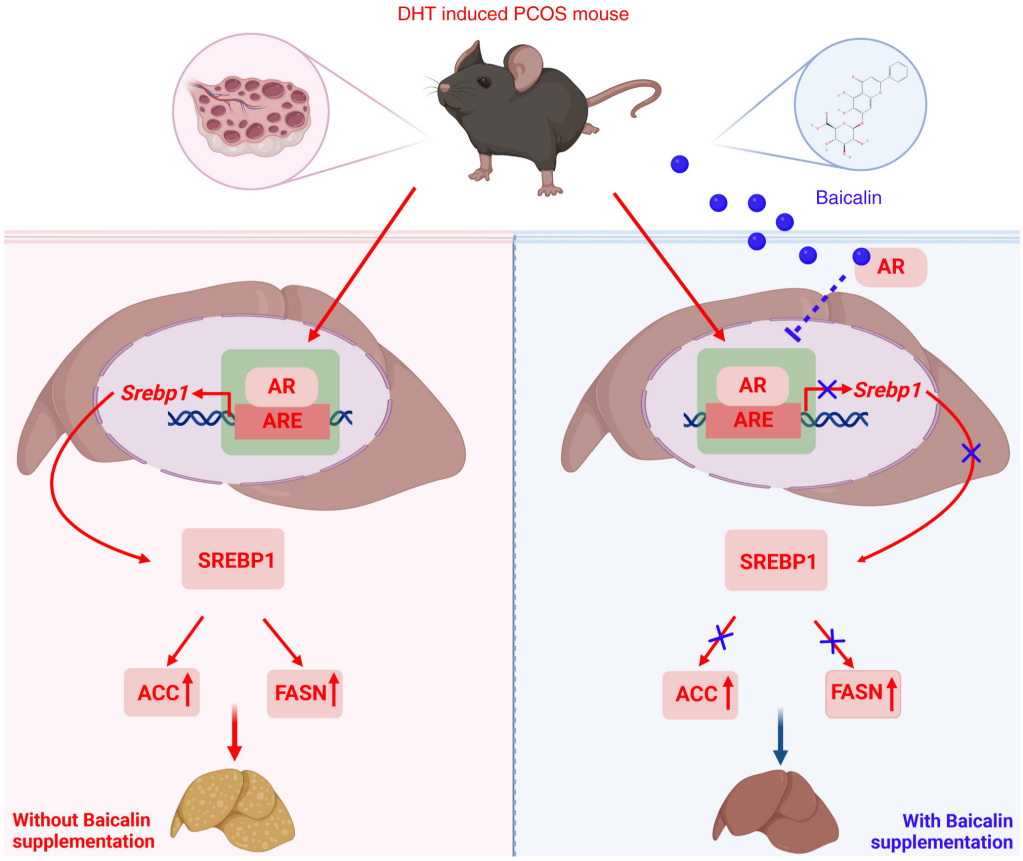

Figure 8. Proposed mechanism by which BA ameliorates PCOS-associated NAFLD via the AR/SREBP1 signaling axis. BA binds to AR and inhibits its transcriptional activity, thereby downregulating the AR-mediated activation of SREBP1. This suppression leads to decreased expression of key lipogenic enzymes, including FASN and ACC, resulting in reduced hepatic lipogenesis. Through this pathway, BA alleviates hepatic steatosis and metabolic dysfunction in a DHT-induced mouse model of PCOS with NAFLD. BA, baicalin; PCOS, polycystic ovary syndrome; NAFLD, non-alcoholic fatty liver disease; AR, androgen receptor; SREBP1, sterol regulatory element-binding protein 1; FASN, fatty acid synthase; ACC, acetyl-CoA carboxylase; DHT, dihydrotestosterone.

BA, a flavonoid derived from *Scutellaria baicalensis*, possesses anti-inflammatory, antioxidant and lipid-lowering properties, highlighting its potential as a candidate for metabolic disorder management, particularly NAFLD. Results of previous studies revealed that BA mitigates hepatic steatosis through reducing lipogenesis and enhancing lipid oxidation, primarily through AMPK activation and the downregulation of key lipogenic genes (37,38). In addition, BA suppressed pro-inflammatory cytokines via NF-κB and NLRP3 inhibition, thereby reducing liver injury and fibrosis (39,40).

While these mechanisms contribute to the hepatoprotective effects of BA, its role in PCOS-associated NAFLD remains to be fully elucidated. The majority of conventional PCOS treatments primarily target insulin resistance or ovarian dysfunction,

often overlooking the contribution of hyperandrogenism-driven hepatic lipogenesis (41). The present study addressed this gap by introducing a novel therapeutic dimension; namely, direct AR inhibition, specifically targeting androgen-induced hepatic lipid accumulation, which is increasingly recognized as a key pathological driver in this subset of NAFLD (2). Compared with previous studies that are mainly focused on BA in the indirect modulation of androgenic pathways (17,42), the present study provided direct biochemical evidence that BA physically binds to AR and inhibits its transcriptional activity, as demonstrated by ITC assays and luciferase reporter experiments. These findings complement and extend earlier reports suggesting that BA suppresses AR nuclear translocation and downstream signaling (19,42), while offering a more precise mechanistic insight into its anti-androgenic effects.

To the best of the authors' knowledge, the present study was the first to investigate the use of BA in a PCOS-NAFLD context, thereby establishing its relevance in a clinically important intersection of metabolic and endocrine dysfunction. In contrast to synthetic AR antagonists, such as flutamide, which are often associated with hepatotoxicity, teratogenicity or acquired resistance (11,12), BA has demonstrated a favorable safety profile. This is supported by its use in Traditional Chinese Medicine (43,44) and when administered for gestational indications during pregnancy (45,46). These factors highlight the potential for safer, long-term use in females of reproductive age. Moreover, the anti-androgenic properties of BA are well-established in classical androgen-responsive tissues (17,19,42); thus, these may also extend to key metabolic and endocrine organs implicated in PCOS pathophysiology, including adipose tissue, skeletal muscle and the ovary. Such broader endocrine modulation has the potential to influence body fat distribution, enhance insulin sensitivity and regulate ovarian steroidogenesis, thereby offering a multifaceted therapeutic benefit for the complex metabolic disturbances associated with PCOS.

Through integrating a focused disease model, direct molecular targeting and translational relevance, the present study furthered the current mechanistic understanding of BA on AR signaling and expanded the potential therapeutic application beyond general NAFLD to encompass hyperandrogenism-associated liver and metabolic disorders.

However, the present study exhibited limitations. Notably, BA-AR binding was only demonstrated *in vitro* via ICT; thus, further *in vivo* assays under physiological androgen levels are required to confirm the observed interaction. Moreover, although the present data suggested that BA suppresses AR-mediated SREBP1 activation, direct verification with AR chromatinbinding or SREBP1 reporter assays are also required. Notably, results obtained from the DHT-induced PCOS-NAFLD mouse model may not fully extrapolate to human pathology; thus, clinical investigations are essential for further validation. Furthermore, the limited sample size may have introduced variability and contributed to potential deviations in the results, underscoring the importance of larger cohorts in future studies to improve statistical robustness. In addition, hyperandrogenic signaling involves numerous coregulators beyond the AR/SREBP1 axis. Thus, network-level studies are required to identify additional pathways that may contribute to the therapeutic effects of BA.

For the implementation of BA in clinical practice, future investigations should focus on optimizing human dosing, pharmacokinetics and liver-targeted delivery, using nanocarriers or pro-drug formulations, where appropriate. Subsequent studies should also evaluate BA in combination with insulin-sensitizing or other metabolic agents to assess additive efficacy. Notably, biomarker-driven clinical trials are also required to verify sustained endocrine and cardiometabolic benefits in females with PCOS. Parallel structure-activity screening of BA analogues and associated flavonoids may identify compounds with greater potency or selectivity. In addition, integrated multiomics analyses of adipose, muscle and gut will delineate the extrahepatic actions of BA and uncover additional metabolic targets, providing a more comprehensive therapeutic profile.

Although the hepatoprotective and anti-androgenic properties of BA have been documented in other pathophysiological contexts, to the best of the authors' knowledge, the present study is the first to demonstrate the BA-mediated direct inhibition of the AR/SREBP1 axis in PCOS-associated NAFLD (Fig. 8). In conclusion, results of the present study provided a mechanistic foundation for BA in counteracting hyperandrogen-driven hepatic steatosis, highlighting its potential as a therapeutic candidate that addresses both the reproductive and metabolic complications of PCOS.

Acknowledgements

The authors thank Professor Guocan Yu (Department of Chemistry, Tsinghua University, China) for his invaluable guidance throughout the experiments. The authors are also grateful to Professor Wei Shi's laboratory (School of Environment, Nanjing University, China) for generously providing the MDA-kb2 cell line. The authors acknowledge Dr Siyuan Shen, Dr Zhuangchou Han and colleagues from LC Bio Technology Co., Ltd. (China) for their assistance with sequencing and bioinformatics analysis.

Funding

The present study was supported by Basic Research Project of Hangzhou Medical College (grant no. KYZD202202), Zhejiang Provincial Natural Science Foundation of China (grant no. LTGY24H150006) and Zhejiang Provincial Program for the Cultivation of High-Level Innovative Health Talents (grant no. 1WJW2022004).

Availability of data and materials

The RNA-seq data generated from this study can be obtained from NCBI GEO database with accession number GSE305214 or at the following URL: https://www.ncbi.nlm.nih.gov/geo/query/acc.cgi?acc=GSE305214. Other data supporting the findings of this study may be requested from the corresponding author.

Authors' contributions

BHJ, HX and LBQ designed the study. BHJ and HX wrote the first draft of the manuscript. ZYZ, YHF and CYJ performed

data curation and validation. BHJ, ZYZ and CYJ conducted visualization. YHF and SLQ performed methodology design and validation. HX carried out investigation. SLQ conducted formal analysis. BHJ, HX, ZYZ and CYX were responsible for project administration. CYX provided resources. XHF and LBQ supervised the study and revised the manuscript. LBQ acquired funding. BHJ and LBQ confirmed the authenticity of all the raw data. All authors read and approved the final version of the manuscript.

Ethics approval and consent to participate

The present study was approved by the Ethical Committee of Zhejiang Provincial Peoples' Hospital (approval no. 20240708135746975190).

Patient consent for publication

Not applicable.

Competing interests

The authors declare that they have no competing interests.

References

1. Siddiqui S, Mateen S, Ahmad R and Moin S: A brief insight into the etiology, genetics, and immunology of polycystic ovarian syndrome (PCOS). J Assist Reprod Genet 39: 2439-2473, 2022.
2. Xu Q, Zhang J, Lu Y and Wu L: Association of metabolic-dysfunction associated steatotic liver disease with polycystic ovary syndrome. iScience 27: 108783, 2024.
3. Vidal-Cevallos P, Mijangos-Trejo A, Uribe M and Tapia NC: The interlink between metabolic-associated fatty liver disease and polycystic ovary syndrome. Endocrinol Metab Clin North Am 52: 533-545, 2023.
4. Paschou SA, Polyzos SA, Anagnostis P, Goulis DG, Kanaka-Gantenbein C, Lambrinoudaki I, Georgopoulos NA and Vryonidou A: Nonalcoholic fatty liver disease in women with polycystic ovary syndrome. Endocrine 67: 1-8, 2020.
5. Kumarendran B, O'Reilly MW, Manolopoulos KN, Toulis KA, Gokhale KM, Sitch AJ, Wijeyaratne CN, Coomarasamy A, Arlt W and Nirantharakumar K: Polycystic ovary syndrome, androgen excess, and the risk of nonalcoholic fatty liver disease in women: A longitudinal study based on a United Kingdom primary care database. PLoS Med 15: e1002542, 2018.
6. Wu J, Yao XY, Shi RX, Liu SF and Wang XY: A potential link between polycystic ovary syndrome and non-alcoholic fatty liver disease: an update meta-analysis. Reprod Health 15: 77, 2018.
7. Younossi ZM, Blissett D, Blissett R, Henry L, Stepanova M, Younossi Y, Racila A, Hunt S and Beckerman R: The economic and clinical burden of nonalcoholic fatty liver disease in the United States and Europe. Hepatology 64: 1577-1586, 2016.
8. Swinnen JV, Ulrix W, Heyns W and Verhoeven G: Coordinate regulation of lipogenic gene expression by androgens: Evidence for a cascade mechanism involving sterol regulatory element binding proteins. Proc Natl Acad Sci USA 94: 12975-12980, 1997.
9. Li N, Li X, Ding Y, Liu X, Diggle K, Kisseleva T and Brenner DA: SREBP regulation of lipid metabolism in liver disease, and therapeutic strategies. Biomedicines 11: 3280, 2023.
10. Seidu T, McWhorter P, Myer J, Alamgir R, Eregha N, Bogle D, Lofton T, Ecelbarger C and Andrisse S: DHT causes liver steatosis via transcriptional regulation of SCAP in normal weight female mice. J Endocrinol 250: 49-65, 2021.
11. Matsumoto H, Yamamoto Y, Shiota M, Kuruma H, Beraldi E, Matsuyama H, Zoubeidi A and Gleave M: Cotargeting androgen receptor and clusterin delays castrate-resistant prostate cancer progression by inhibiting adaptive stress response and AR stability. Cancer Res 73: 5206-5217, 2013.
12. Saxena N, Beraldi E, Fazli L, Somasekharan SP, Adomat H, Zhang F, Molokwu C, Gleave A, Nappi L, Nguyen K, *et al*: Androgen receptor (AR) antagonism triggers acute succinate-mediated adaptive responses to reactivate AR signaling. EMBO Mol Med 13: e13427, 2021.
13. Magni P, Macchi C, Morlotti B, Sirtori CR and Ruscica M: Risk identification and possible countermeasures for muscle adverse effects during statin therapy. Eur J Intern Med 26: 82-88, 2015.
14. Yaribeygi H, Maleki M, Butler AE, Jamialahmadi T and Sahebkar A: New insights into cellular links between sodium-glucose cotransporter-2 inhibitors and ketogenesis. J Cell Biochem 123: 1879-1890, 2022.
15. Hu Q, Zhang W, Wu Z, Tian X, Xiang J, Li L, Li Z, Peng X, Wei S, Ma X, *et al*: Baicalin and the liver-gut system: Pharmacological bases explaining its therapeutic effects. Pharmacol Res 165: 105444, 2021.
16. Dai J, Liang K, Zhao S, Jia W, Liu Y, Wu H, Lv J, Cao C, Chen T, Zhuang S, *et al*: Chemoproteomics reveals baicalin activates hepatic CPT1 to ameliorate diet-induced obesity and hepatic steatosis. Proc Natl Acad Sci USA 115: E5896-e5905, 2018.
17. Jin BR and An HJ: Baicalin alleviates benign prostate hyperplasia through androgen-dependent apoptosis. Aging (Albany NY) 12: 2142-2155, 2020.
18. Chan FL, Choi HL, Chen ZY, Chan PS and Huang Y: Induction of apoptosis in prostate cancer cell lines by a flavonoid, baicalin. Cancer Lett 160: 219-228, 2000.
19. Kim AR, Kim SN, Jung IK, Kim HH, Park YH and Park WS: The inhibitory effect of Scutellaria baicalensis extract and its active compound, baicalin, on the translocation of the androgen receptor with implications for preventing androgenetic alopecia. Planta Med 80: 153-158, 2014.
20. Xu X, Xu X, Wang X and Shen L: Baicalin suppress the development of polycystic ovary syndrome via regulating the miR-874-3p/FOXO3 and miR-144/FOXO1 axis. Pharm Biol 61: 878-885, 2023.
21. Percie du Sert N, Hurst V, Ahluwalia A, Alam S, Avey MT, Baker M, Browne WJ, Clark A, Cuthill IC, Dirnagl U, *et al*: The ARRIVE guidelines 2.0: Updated guidelines for reporting animal research. Br J Pharmacol 177: 3617-3624, 2020.
22. Jin J, Ma Y, Tong X, Yang W, Dai Y, Pan Y, Ren P, Liu L, Fan HY, Zhang Y, *et al*: Metformin inhibits testosterone-induced endoplasmic reticulum stress in ovarian granulosa cells via inactivation of p38 MAPK. Hum Reprod 35: 1145-1158, 2020.
23. Aflatounian A, Paris VR, Richani D, Edwards MC, Cochran BJ, Ledger WL, Gilchrist RB, Bertoldo MJ, Wu LE and Walters KA: Declining muscle NAD(+) in a hyperandrogenism PCOS mouse model: Possible role in metabolic dysregulation. Mol Metab 65: 101583, 2022.
24. American Veterinary Medical Association: AVMA Guidelines for the Euthanasia of Animals: 2020 edition. American Veterinary Medical Association, Schaumburg, IL, 2020.
25. McLean AC, Valenzuela N, Fai S and Bennett SA: Performing vaginal lavage, crystal violet staining, and vaginal cytological evaluation for mouse estrous cycle staging identification. J Vis Exp 15: e4389, 2012.
26. Ashburner M, Ball CA, Blake JA, Botstein D, Butler H, Cherry JM, Davis AP, Dolinski K, Dwight SS, Eppig JT, *et al*: Gene ontology: Tool for the unification of biology. The Gene Ontology Consortium. Nat Genet 25: 25-29, 2000.
27. Kanehisa M and Goto S: KEGG: kyoto encyclopedia of genes and genomes. Nucleic Acids Res 28: 27-30, 2000.
28. Yu G, Wang LG, Han Y and He QY: ClusterProfiler: An R package for comparing biological themes among gene clusters. Omics 16: 284-287, 2012.
29. Livak KJ and Schmittgen TD: Analysis of relative gene expression data using real-time quantitative PCR and the 2(-Delta Delta C(T)) Method. Methods 25: 402-408, 2001.
30. McRae JM, Falconer RJ and Kennedy JA: Thermodynamics of grape and wine tannin interaction with polyproline: implications for red wine astringency. J Agric Food Chem 58: 12510-12518, 2010.
31. Sato R: Sterol metabolism and SREBP activation. Arch Biochem Biophys 501: 177-181, 2010.
32. Audet-Walsh É, Vernier M, Yee T, Laflamme C, Li S, Chen Y and Giguère V: SREBF1 activity is regulated by an AR/mTOR nuclear axis in prostate cancer. Mol Cancer Res 16: 1396-1405, 2018.
33. Singh RK, Kumar S, Tomar MS, Verma PK, Kumar A, Kumar S, Kumar N, Singh JP and Acharya A: Putative role of natural products as protein kinase C modulator in different disease conditions. Daru 29: 397-414, 2021.

34. Barber TM, Kabisch S, Randeva HS, Pfeiffer AFH and Weickert MO: Implications of resveratrol in obesity and insulin resistance: A state-of-the-art review. Nutrients 14: 2870, 2022.
35. He S, He X, Pan S and Jiang W: Exploring the mechanism of chuanxiong rhizoma against thrombosis based on network pharmacology, molecular docking and experimental verification. Molecules 28: 6702, 2023.
36. Hu X, Shi W, Wei S, Zhang X and Yu H: Identification of (anti-) androgenic activities and risks of sludges from industrial and domestic wastewater treatment plants. Environ Pollut 268: 115716, 2021.
37. Guo HX, Liu DH, Ma Y, Liu JF, Wang Y, Du ZY, Wang X, Shen JK and Peng HL: Long-term baicalin administration ameliorates metabolic disorders and hepatic steatosis in rats given a high-fat diet. Acta Pharmacol Sin 30: 1505-1512, 2009.
38. Gao Y, Liu J, Hao Z, Sun N, Guo J, Zheng X, Sun P, Yin W, Fan K and Li H: Baicalin ameliorates high fat diet-induced nonalcoholic fatty liver disease in mice via adenosine monophosphate-activated protein kinase-mediated regulation of SREBP1/Nrf2/NF-κB signaling pathways. Phytother Res 37: 2405-2418, 2023.
39. Shi H, Qiao F, Lu W, Huang K, Wen Y, Ye L and Chen Y: Baicalin improved hepatic injury of NASH by regulating NRF2/HO-1/NRLP3 pathway. Eur J Pharmacol 934: 175270, 2022.
40. Zhang J, Zhang H, Deng X, Zhang N, Liu B, Xin S, Li G and Xu K: Baicalin attenuates non-alcoholic steatohepatitis by suppressing key regulators of lipid metabolism, inflammation and fibrosis in mice. Life Sci 192: 46-54, 2018.
41. Armanini D, Boscaro M, Bordin L and Sabbadin C: Controversies in the pathogenesis, diagnosis and treatment of PCOS: Focus on insulin resistance, inflammation, and hyperandrogenism. Int J Mol Sci 23: 4110, 2022.
42. Chen S, Ruan Q, Bedner E, Deptala A, Wang X, Hsieh TC, Traganos F and Darzynkiewicz Z: Effects of the flavonoid baicalin and its metabolite baicalein on androgen receptor expression, cell cycle progression and apoptosis of prostate cancer cell lines. Cell Prolif 34: 293-304, 2001.
43. Wang L, Feng T, Su Z, Pi C, Wei Y and Zhao L: Latest research progress on anticancer effect of baicalin and its aglycone baicalein. Arch Pharm Res 45: 535-557, 2022.
44. Zhou HC, Du R, Wang H, Zeng FL, Shi K, Li JM and Zong Y: Advance in studies on pharmacokinetics of baicalin. Zhongguo Zhong Yao Za Zhi 43: 684-688, 2018, (In Chinese).
45. Lu JQ, Luo ZY, Sun C, Wang SM, Sun D, Huang RJ, Yang X, Ding Y and Wang G: Baicalin administration could rescue high glucose-induced craniofacial skeleton malformation by regulating neural crest development. Front Pharmacol 15: 1295356, 2024.
46. Deng L, Jin Y, Zheng X, Yang Y, Feng Y, Zhou H and Zeng Q: Pharmacological and toxicological characteristics of baicalin in preventing spontaneous abortion and recurrent pregnancy loss: A multi-level critical review. Heliyon 10: e38633, 2024.